

Soft Matter

Accepted Manuscript



This is an *Accepted Manuscript*, which has been through the Royal Society of Chemistry peer review process and has been accepted for publication.

Accepted Manuscripts are published online shortly after acceptance, before technical editing, formatting and proof reading. Using this free service, authors can make their results available to the community, in citable form, before we publish the edited article. We will replace this *Accepted Manuscript* with the edited and formatted *Advance Article* as soon as it is available.

You can find more information about *Accepted Manuscripts* in the [Information for Authors](#).

Please note that technical editing may introduce minor changes to the text and/or graphics, which may alter content. The journal's standard [Terms & Conditions](#) and the [Ethical guidelines](#) still apply. In no event shall the Royal Society of Chemistry be held responsible for any errors or omissions in this *Accepted Manuscript* or any consequences arising from the use of any information it contains.

Interfacial Rheology of Polymer/Carbon Nanotube Films Co-Assembled at the Oil/Water Interface

Tao Feng¹, David A. Hoagland^{1*}, Thomas P. Russell^{1,2,3*}

¹Polymer Science and Engineering Department, University of Massachusetts at Amherst, Amherst, 01003, USA

²Materials Sciences Division, Lawrence Berkeley National Laboratory, Berkeley, California 94720, USA

³WPI—Advanced Institute for Materials Research (WPI-AIMR), Tohoku University, 2-1-1 Katahira, Aoba, Sendai 980-8577, Japan

Abstract

At appropriate conditions, water-dispersed acid-functionalized single-walled carbon nanotubes (SWCNTs) co-assemble at the oil/water interface with toluene-dissolved amine-terminated polystyrene (PS-NH₂) to form composite thin films displaying pronounced interfacial viscoelasticity. To probe this viscoelasticity, the films were examined under dilatational deformations of pendant drop tensiometry/rheometry, with storage and loss moduli recorded against frequency ω ($0.003 < \omega < 3$ Hz) and time-dependent relaxation modulus recorded against time t ($0.2 < t < 2,000$ s). Without the SWCNTs, PS-NH₂-decorated interfaces have little dilatational stiffness, i.e., low storage modulus, but their stiffness grows as SWCNTs are added, reaching 50-100 mN/m at large ω . Two characteristic relaxation processes are identified in the composite films: a fast process ($\omega \sim 0.1$ - 0.2 Hz) attributable to local structural relaxation of confined PS-NH₂ and a slow process ($t \sim 300$ - $2,000$ s) attributable to component adsorption/desorption (or attachment/detachment). Among the variables that affect positions and strengths of these relaxations are SWCNT and PS-NH₂ bulk concentrations as well as water phase pH. In frequency or timescale ranges intermediate between the two relaxations, the co-assembled films display “soft-glass” behavior, with the storage and loss moduli characterized by nearly equal power-law exponents. The relaxation modulus, better able to probe terminal behavior, eventually decays to zero, revealing that the films are fundamentally fluid-like due to the slow relaxation, and in support of this conclusion, large strain compression-induced film wrinkles disappear at large t .

Key Words: carbon nanotubes, interfacial assembly, interfacial rheology, “salt-bridge” interactions, interfacial films

Introduction

The high water permeability of single-walled carbon nanotubes (SWCNTs) motivates interest in SWCNT/polymer composite membranes for water desalination, water purification, and forward osmosis power generation¹⁻⁵. Making the composite membranes at a liquid/liquid interface has obvious economic benefits but also poses general, fundamental questions about interfacial nanoparticle assembly. Composite thin-films comprised of inorganic nanoparticles⁶⁻⁹, carbon nanotubes^{10, 11} and graphene sheets¹², have been realized by assembly at liquid/liquid or liquid/air interfaces, via either spontaneous segregation or cooperative association with a surfactant¹³⁻¹⁵. A different approach was recently described, one that drives carboxyl-containing (i.e., oxidized) SWCNTs dispersed in water to the oil/water interface through the agency of an oil-soluble, amine-containing polymers dispersed in oil¹⁰. The rheology of the new composite films, intimately connected to their processing and membrane properties, remains unexplored, framing the topic of the current contribution. The principles uncovered in this study should apply to composite films assembled in other ways or containing different components.

Previous investigations of rheology at liquid/liquid interfaces extended to films containing nanoparticles^{16, 17}, low molecular weight surfactants¹⁸, synthetic and bio-polymers¹⁹⁻²³, tiled graphene oxide sheets²⁴, colloids²⁵, and ellipsoidal particle assemblies²⁶. Rheological properties varied significantly by system, with fluid-like, gel-like, and solid-like responses reported along with various relaxation mechanisms^{19, 20, 22, 27}. Ravera et al. studied the solid-like films created at an oil/water interface when silica nanoparticles in water were mixed with cetyltrimethylammonium bromide (CTAB) and fatty amines^{16, 18, 28}. Krishnaswamy et al. demonstrated the soft-glass nature of Ag nanoparticle monolayers formed at the toluene/water interface¹⁷. Diez-Pascual et al. observed that block copolymer films at the air-water interface relax by adsorption/desorption processes well described by the classic Lucassen-van de Tempel model¹⁹. The hydrophobically modified polyacrylamide films studied by Wang et al. at the oil/water interface displayed two relaxations, a fast process attributed to adsorption/desorption and a slow relaxation attributed to polymer conformational changes²⁰. Films of asphaltene, with stronger intermolecular interactions, formed films with soft-glass character²⁹. At the air/water interface, Freer et al. demonstrated a dominantly viscous response for an adsorbed β -casein film, but for an analogous lysozyme film, they reported dominantly elastic response, the difference between the proteins explained in terms of the interfacial network produced at long times by lysozyme denaturation^{22, 27}. For colloids with ellipsoidal geometry, Madivala²⁶ et al. demonstrated that highly elastic monolayers can be generated by tailoring surface charge and particle wetting properties.

Our interfacial film strategy is simple¹⁰: an oil dissolving an amine-functionalized polymer is contacted with water dispersing a nanomaterial of modest anionic charge. Under an interface-localized attraction between amine and acid, the solutes co-assemble, creating a film of tens-of-nanometer thickness and an interface of dramatically lowered interfacial tension. Importantly, the polymer must be sufficiently hydrophobic to remain in the oil phase and the nanomaterial must be sufficiently hydrophilic to remain in the water phase. The two consequently meet only at/near the interface, where the acid-amine interaction, termed salt-bridging, combines aspects of

electrostatic attraction and hydrogen bonding. The rheology of the composite interfacial films has not previously been assessed. In fact, whether the films are fluid or solid remains unclear. Long-lived wrinkles, observed on the drop interface when the drop volume was diminished, demonstrated that the films possess transient, or even permanent, solid-like character.

Interfacial dilatational rheology probes the stress-strain response of films at liquid/liquid and air/liquid interfaces under stress-strain protocols similar to those of bulk rheology, i.e., under oscillation, step strain, etc. The so-determined interfacial rheological properties have been correlated with emulsion and foam stability³⁰. When a fluid-fluid interface is driven out of equilibrium by an areal expansion or contraction that creates dilatational strain, various relaxation processes can return the interface to equilibrium. Alongside the structural relaxations in the interfacial layer itself, reflecting changes in molecular orientation/aggregation/conformation/packing, relaxations can emanate from exchanges of the interfacial components with the surrounding bulk phases. Interfacial shear rheology is a related experiment that, at low strain, manifests many of the same relaxations.

In the oscillatory dilatational rheology experiment, if the area change is small enough, i.e., if the interfacial dilatational strain falls within the linear viscoelastic regime, rheological properties are captured in the frequency ω -dependent dilatational complex modulus $E^*(\omega)$, which decomposes into its real (storage) and imaginary (loss) components, $E'(\omega)$ and $E''(\omega)$, respectively, from which the phase angle δ is determined,

$$E^*(\omega) = E'(\omega) + i\omega E''(\omega) \quad \tan\delta(\omega) = E''(\omega)/E'(\omega)$$

These two-dimensional dilatational moduli have fundamental units of mass/time², alternately expressed energy/area or force/length, combinations carrying the same fundamental units as interfacial tension. Indeed, $E^*(\omega)$ is calculated

$$E^*(\omega) = \frac{d\gamma}{d\ln A/A_0}$$

as the area A sinusoidally oscillates with amplitude ΔA about initial area A_0 ,

$$A(t) = A_0 + \Delta A \exp(i\omega t)$$

and the measured surface tension $\gamma(t)$ oscillates about the static surface tension γ_0 with amplitude $\Delta\gamma(\omega)$,

$$\gamma(t) = \gamma_0 + \Delta\gamma(\omega)\exp[i(\omega t + \delta(\omega))]$$

Interfacial layers are not perfectly two-dimensional, and acknowledging a layer of finite thickness and uniform properties, these moduli are proportional to thickness.

Interfacial dilatational stress relaxation experiments are more effective than interfacial dynamics experiments at probing terminal regime rheology, defined by linear viscoelastic behaviors at large enough t , or small enough ω , to encompass all interfacial relaxation processes. In particular, the presence of an equilibrium modulus in a shear stress relaxation experiment unequivocally determines whether an interfacial layer is fundamentally fluid-like or solid-like, with only the

latter supporting such a stress. In a pendant drop experiment, an infinitesimal areal expansion or contraction at $t=0$ puts the interface under steady dilatational strain (not shear), with the subsequent stress relaxation monitored through $\gamma(t)$,

$$E(t) = \frac{|\gamma(t) - \gamma_0|}{\Delta A/A_0}$$

where $E(t)$ is the dilatational relaxation modulus. Accurate measurements can be taken out to $\sim 10,000$ s or longer, probing relaxation processes more than an order-of-magnitude slower than possible in the analogous interfacial dynamics experiment. For interfacial oscillatory and stress relaxation experiments conducted in the linear viscoelastic regime, compositions of the interfacial film and the two surrounding bulk phases remain essentially constant.

Interfacial tensiometer experiments performed after finite changes to bulk composition(s) further elucidate the kinetics of interfacial film assembly/disassembly, providing related but non-rheological insights into film relaxation processes, particularly those associated with component adsorption/desorption or attachment/detachment. Two distinct experiments are most revealing: (i) the monitoring of $\gamma(t)$ for a freshly created interface, which probes film assembly kinetics, and (ii) the monitoring of $\gamma(t)$ for an equilibrated interface immediately after a reduction of bulk phase concentration(s), which probes film disassembly kinetics. For the latter, most convenient is the exchange of solution for pure solvent in the liquid surrounding the test droplet, this exchange driving film disassembly and thereby revealing whether assembly/disassembly is reversible, as expected for a soluble fluid-like film.

Experimental Section

Materials. Pristine SWCNTs at nanotube purity $>90\%$ were purchased from Nanocs Inc. (cat. no. CNTS01); diameters and lengths ranged, respectively, from 2 to 10 nm and 50 nm to several μm . Sulfuric acid (98%) and nitric acid (70%) along with reagent grade toluene were purchased from Fisher Scientific Inc. and used as received. Monoamine-terminated polystyrene (PS-NH₂) was purchased from Polymer Source Inc. ($M_n=2,800$ g/mol, $M_w/M_n=1.3$, cat. no. P5147-SNH2), and gold nanoparticles (Au NPs) (5-nm diameter, citrate acid-functionalized, 0.05 mg/ml concentration) were purchased from nanoComposix (product no. AUPN5-25M).

SWCNT Treatment. Acid functionalization of SWCNTs followed previous procedures¹⁰. Briefly, purchased SWCNTs were treated by an acid “cutting” and oxidation procedure in which 20 mg of dispersed SWCNTs were vigorously sonicated at 45 °C for 6 h in a mixture of 60 ml sulfuric acid and 20 ml nitric acid. After this treatment, the suspension was diluted with 500 ml of deionized water and filtered through 200-nm pore size microporous nylon membranes (Pall Corporation, cat. no. 66602) to isolate the SWCNTs, which readily redispersed (and remained stable for months) in de-ionized water. Analyzing dynamic light scattering data by the slender body hydrodynamic theory for rods, the length distribution for the acid-treated SWCNTs spanned 20-100 nm with a peak at 30 nm. SWCNT morphology was further assessed by transmission electron microscopy, finding the average tube diameter to be 8 ± 2 nm, a value

consistent with the 2-10 nm untreated diameter specified by the supplier; the CNTs in TEM images appeared single-walled, although the presence of double- and multi-walled tubes couldn't be discounted, and some amorphous carbon was noted. The SWCNT length distribution wasn't quantified by the microscopy due to SWCNT overlap, but rod-like elements of approximately 100-nm length were apparent. The SWCNT oxidation states were examined by Raman spectroscopy and titration, and the level of oxidized carbon was about 17%, dominantly in the form of carboxyls and phenols, functionalities with pK_a values of 4.5 and 10, respectively.

Interfacial Dilatational Rheology. Interfacial dilatational rheology was performed using a pendant drop tensiometer (Dataphysics, OCA 20) coupled to an oscillation drop generator (Dataphysics, ODG 20) housing a piezoelectric element able to produce changes in drop surface area over broad ranges of ΔA and ω . The tensiometry was calibrated by setting bare water/air and water/toluene interfacial tensions to standard values³¹, and three independent measurements were performed at each measurement condition such that typical differences between independent measurements were less than ~ 0.5 mN/m. In oscillatory experiments, as illustrated in Figure S1, a fresh SWCNT-containing water drop was created inside a toluene solution of PS-NH₂, and before the start of testing, with drop volume fixed, interfacial assembly was allowed to reach steady-state, a condition deduced by the experiments described in the next section. The bulk SWCNT concentration C_{SWCNT} varied from 0.005 to 0.08 mg/ml, and the bulk PS-NH₂ concentration C_{PS-NH_2} varied from 0.001 to 0.3 mg/ml. All SWCNTs originated from one treatment batch, and so, their mass concentrations and volume fractions are proportional, the two measures of bulk SWCNT concentration related by a constant SWCNT density³². Analysis of a video record of drop shape provided γ as a function of t , which in conjunction with A/A_0 , allowed calculation of E^* . With the linear viscoelastic regime verified to continue past 8% strain, for adequate signal-to-noise $\Delta A/A_0$ was set to 3.5%, while ω spanned 0.003 to 2 Hz, the practical upper and low limits to tensiometer operation. Stress relaxation experiments, also with $\Delta A/A_0$ set to 3.5%, were performed similarly, using capabilities of the tensiometer to implement a step areal strain.

Pendant Drop Tensiometry to Assess Interfacial Film Assembly/Disassembly. To evaluate the timescale for interfacial layer assembly as a function of C_{SWCNT} , using the same tensiometer, $\gamma(t)$ was monitored to near steady state for a water drop was created at $t=0$. This drop (10 μ L nominal volume, 0.005 mg/ml $< C_{SWCNT} < 0.08$ mg/ml) was injected into a much larger (2.5 ml) reservoir of toluene at constant C_{PS-NH_2} (0.2 mg/ml). Likewise, as indicated in Figure S2, to evaluate the timescale for interfacial layer disassembly, $\gamma(t)$ was monitored for a previously equilibrated drop (0.005 mg/ml $< C_{SWCNT} < 0.08$ mg/ml) by replacing the PS-NH₂-containing reservoir fluid ($C_{PS-NH_2}=0.2$ mg/ml) with pure toluene at $t=0$. Fluid exchange was accomplished by gravity flow between the reservoir inlet and outlet, and about 6 reservoir fluid volumes were exchanged at the start of an experiment. During this exchange, the Reynolds and Capillary numbers were small enough to hold the drop shape profile constant.

Results and Discussion

Under appropriate conditions, strong salt bridging between oxidized SWCNTs dispersed in water and low molecular weight PS-NH₂ dissolved in oil (toluene) produces robust interfacial films and dramatic decreases in water/oil interfacial tension. The coupling is strongly pH-dependent, reflecting the *pKa* of the carboxyls of the oxidized SWCNTs; at a pH much above the *pKa*, the mutual electrostatic repulsions among the multiply charged SWCNTs interfere with their segregation to the interface, and films are weak and the interfacial tension change caused by co-assembly is attenuated. Interfacial tension is also affected by C_{PS-NH_2} and C_{SWCNT} . Conditions conducive to the creation of robust films mainly reflect interactions perpendicular to the interface, whereas interfacial rheology more immediately reflects interactions within the plane of the interface. Even casual observations reveal that some of the films are strongly viscoelastic.

Interfacial Viscoelasticity: Trends in the Dynamics Experiments. Figure 1 presents representative trends in $E'(\omega)$ and $E''(\omega)$ after steady state interfacial assembly at $C_{SWCNT}=0.02$ mg/ml, $C_{PS-NH_2}=0.2$ mg/ml, and pH=3.0, conditions that support formation of robust, homogeneous, and isotropic films with $\gamma_0 \sim 11.3$ mN/m, significantly less than the 34 mN/m value for the bare toluene-water interface; the figure's inset shows the underlying rheology data at $\omega=0.01$ Hz. The film thickness, estimated by mechanical profilometry after transfer from the interface and rapid drying on a silicon wafer, is ~ 20 nm, less than the average cut SWCNT length. Drying probably alters SWCNT orientation, and may cause SWCNT aggregation, but given the film thickness, the SWCNTs in the wet film clearly must preferentially align in the film plane or protrude from the film surface. The fully extended contour length of PS-NH₂ is ~ 7 nm. Taken together, these lengths point to a complex film nanostructure, consistent with the SEM image of the dried film's "bird's nest"-like morphology shown in Figure S3. Figure 1 also plots $E'(\omega)$ and $E''(\omega)$ at the same assembly condition except with SWCNTs absent from the aqueous phase. For this control experiment, $\gamma_0 \sim 27$ mN/m, much closer to $\gamma_0 \sim 34$ mN/m, indicating a sparser, or weaker, film than in the presence of SWCNTs. PS-NH₂ is essentially a weak surfactant dissolved above its critical micelle concentration, ~ 0.08 mg/ml.

For the control film, $E'(\omega)$ and $E''(\omega)$ are relatively small, and both increase slowly with ω . At the largest ω reached, $\sim 1-2$ Hz, where $E'(\omega)$ of both co-assembled and control films trend toward a ω -independent plateau, $E'(\omega)$ for the co-assembled film is more than 5 times greater than for the control film. This enhancement reflects (i) mechanical reinforcement conveyed by SWCNTs, (ii) enhanced rigidity of a denser polystyrene interface phase unable to relax at short timescales, and/or (iii) augmented PS-NH₂ at the interface when SWCNT binding sites are available. Trends of $E'(\omega)$ at low ω for the co-assembled and control films are less obvious (see next section), but $E'(\omega)$ falls as ω decreases, and $E''(\omega)$ for both co-assembled and control film is less than $E'(\omega)$. The most striking difference between co-assembled and control films is a pronounced $E''(\omega)$ maximum for the co-assembled film at $\omega \approx 0.1-2$ Hz, a feature coincident with an upward turn in $E'(\omega)$. Neither feature is displayed for the control film. These features establish that the co-assembled film undergoes a significant relaxation in the timescale range $\sim 1-5$ s, a process missing in the pure PS-NH₂ control film, or alternately, with this process shifted to ω above that probed by the experiment.

Interfacial Rheology: Dynamics Experiments at Lower ω . To clarify the lower ω behaviors of co-assembled films and to understand the influence of SWCNTs on film rheology, log-log plots of $E'(\omega)$, $E''(\omega)$ and $\tan\delta(\omega)$ are given in Figure 2 for the same, as well as higher, C_{SWCNT} . The plots are inconsistent with the terminal behavior of a classic Newtonian fluid or classic Hookean solid, i.e., they differ from $E'(\omega)\sim\omega^2$, $E''(\omega)\sim\omega$ for the fluid or $E'(\omega)=constant$, $E''(\omega)\sim\omega$ for the solid³³. Instead, at ω below the relaxation outlined in the last section, $E'(\omega)$ and $E''(\omega)$ roughly trace parallel power-laws for at least one to two decades of ω , and as a consequence, $\tan\delta(\omega)$ for this span is independent of ω . These behaviors can be summarized.

$$E'(\omega)\sim E''(\omega)\sim\omega^n, n = \frac{n\pi}{2}$$

where the power law exponent n is constrained $0 < n < 1$. **Figure 2(c)** establishes that n grows with increasing C_{SWCNT} .

Although measured in bulk shear rather than interfacial dilatation, low ω power laws in $E'(\omega)$ and $E''(\omega)$ for materials intermediate between fluid and solid were first analyzed by Winter and Chambon, who coined the term “critical gel”³⁴. Similar power-law behaviors were observed for other systems, and when repulsive rather than attractive interactions among the components dominate, the term “soft glass” has been assigned instead. Soft glass interfacial films have been characterized by interfacial dynamics rheology,²⁹ with results similar to those reported here. Over regimes of power law viscoelasticity, characteristic material length and time scales for energy dissipation and storage are absent, and a fractal microstructural organization emerges. For the co-assembled interfacial films studied here, the nature of the interactions and morphology are unclear, and ascribing behavior to critical gel or soft glass remains speculative. For the power law region of Figure 2, n rises from ~ 0.25 to ~ 0.5 . Trends of Figure 2 suggest a further ω transition, below the ω range observed, to either fluid or solid terminal behaviors.

Figure 2 displays a systematic shift of the relaxation peak to lower ω as C_{SWCNT} rises, and the tensiometry data for the same systems given in Figure S4 demonstrate that γ_o drifts downward as well, apparently reaching a C_{SWCNT} -independent plateau of $\sim 6-8$ mN/m at $C_{SWCNT}\sim 0.08$ mg/ml. This plateau establishes a saturation of accumulated mass in the interfacial film, and when considered alongside the previously published trends of γ_o with pH, the mutual electrostatic repulsions among the adhered SWCNTs emerges as a likely explanation for such saturation. At low C_{SWCNT} , a significant depletion of SWCNTs from the bulk aqueous phase occurs during their segregation to the interface; for fluorescently labeled SWCNTs, this depletion is revealed by confocal imaging¹⁰.

Origin of the Relaxation Observed in the Dynamics Experiments. As noted in the Introduction, relaxations at a liquid/liquid interface fall into two categories, structural reorganizations within the interface itself and transport processes between the interface and the bulk, basically adsorption/desorption or attachment/detachment. In regard to the latter, an incremental stress supported by an interfacial component is lost upon its desorption/detachment. Further, polymers and nanomaterials co-assembled at an interface can contribute to the interfacial dilatational stress either cooperatively or independently depending on the interaction between the two components. Irreversible SWCNT attachment, for example, can arise in concert

with reversible PS-NH₂ adsorption if all PS-NH₂-SWCNT contacts must break simultaneously for a SWCNT to detach; even with a small individual contact energy, given the large number of contact sites per SWCNT, the probability for SWCNT detachment becomes vanishingly small. In this scenario, which is somewhat analogous to the argument for irreversible physical adsorption of a dissolved flexible polymer to a solid, a long-lived interfacial SWCNT stress contribution manifests interactions with more rapidly relaxed PS-NH₂. Nevertheless, a significant SWCNT stress contribution also requires a mechanism of dilatational stress conveyance among the bound SWCNTs; 2D network formation might be such a conveyance. Other relaxation scenarios can be imagined, but poor knowledge of film morphology and component interactions hinders detailed physical interpretations. The morphology of a soft film at the liquid/liquid interface is difficult to characterize quantitatively *in situ* by standard methods such as scattering and microscopy, especially when the film contains orientable rod-like components (e.g., carbon nanotubes or nanorods). The thin-film transfer technique used in this work, perhaps the best option, can nonetheless distort the morphology. With the interfacial thin-films generated by ellipsoidal particles²⁶, metal nanorods³⁵, or co-assembled nanotube and nanoparticles^{36, 37}, rod-like constituents typically orient preferentially parallel to the interface. Lateral ordering is only observed for well-defined nanorods or nano-ellipsoids upon a compression in the plane of the interface^{26, 38}.

To evaluate the timescale for SWCNT attachment, $\gamma(t)$ was collected as a function of C_{SWCNT} for an initially SWCNT-free water/toluene interface, with the result shown in Figure S4; for this experiment, C_{PS-NH_2} was 0.2 mg/ml. After an initial decrease too fast to be captured in the data, $\gamma(t)$ can be satisfactorily fit to a single exponential time decay, with the fitted decay constant τ varying from 610 s at 0.005 mg/ml to 260 s at 0.08 mg/ml. The immediate drop is consistent with rapid equilibration of the bare interface with PS-NH₂. Given the large difference in PS-NH₂ and SWCNT sizes (mobilities), as well as the dependence of τ on C_{SWCNT} , it is reasonable to attribute the slow $\gamma(t)$ decay to diffusion-controlled attachment of SWCNTs to the interface. The timescale for this process lies well outside the time/frequency range probed in the dynamics experiment. The starting interface for this test was not the same as the SWCNT-equilibrated interfaces of the oscillatory experiments, but timescales of diffusion-controlled (in bulk) SWCNT attachment should not be too dissimilar, and most importantly, τ is orders-of-magnitude too large to correspond to the relaxation process producing the $E''(\omega)$ peaks of Figures 1 and 2.

Likewise, to determine the timescale for PS-NH₂ desorption, possibly different than for PS-NH₂ adsorption, $\gamma(t)$ was collected after abrupt replacement of the PS-NH₂-containing toluene phase (C_{PS-NH_2} = 0.2 mg/ml) with pure toluene; C_{SWCNT} was 0.02 mg/ml, and the recovery in $\gamma(t)$ is plotted in Figure 3. Complete desorption was not achieved in 5000 s, but $\gamma(t)$ mostly recovers over 3000-5000 s, which once again, is much too long to associate with the $E''(\omega)$ peak. The underlying dynamics could be complicated, but it would seem that PS-NH₂ does not desorb fully until SWCNTs are detached.

When the volume of an equilibrated drop is reduced significantly by the abrupt withdrawal of interior fluid, i.e., when the drop interface is subjected to a large amplitude dilatational compression ($\Delta A/A_0 > 50\%$), the surface wrinkles, and in extreme cases, even crumples if the

strain is large enough. Wrinkling recovery after a finite compression is visualized through the image series of the inset to Figure 3. The deduced recovery time, ~ 1300 s, is consistent with the preceding estimates for timescales of detachment/desorption of one, or both, of the co-assembled components. With γ after recovery essentially the same as before compression, ~ 11 mN/m, the excess film mass per area induced by compression was desorbed/detached and fully transported to bulk.

Given that adsorption/desorption (alternately, attachment/detachment) does not seem to be the origin of the ~ 0.1 - 0.2 Hz relaxation, the second possibility, structural rearrangement within the film itself, was explored by replacing SWCNTs with 5 nm-diameter carboxylic acid-functionalized gold nanoparticles (Au NPs). The replacement potentially reveals whether the relaxation dominantly reflects processes intrinsic to polymer (PS-NH₂) or nanomaterial (SWCNT or Au NP). Films made from Au NPs and SWCNTs with PS-NH₂ at the same conditions have similar appearances, but from the geometrical perspective, Au NPs little resemble SWCNTs in shape or size, and so, they will contribute to film rheology differently. Figure S5 demonstrates that Au NP-containing films display viscoelastic behaviors close to those of SWCNT-containing films, and significantly, that Au NP-containing films display an $E''(\omega)$ maximum at ~ 0.2 Hz, the nominal location of the $E''(\omega)$ maximum for SWCNT-containing films. The peak can thus be ascribed to PS-NH₂.

Figure 4 reinforces the attribution of the $E''(\omega)$ peak to PS-NH₂ by showing trends for this peak as C_{PS-NH_2} varies. To help interpret the trends, the figure's inset provides the PS-NH₂ surface excess Γ_{PS-NH_2} as a function of C_{PS-NH_2} measured by the Gibb's absorption isotherm method when SWCNTs are absent from the aqueous phase. Saturation of the interface at $C_{PS-NH_2}=0.08$ mg/ml is evident, consistent with the weak surfactancy of PS-NH₂. With C_{SWCNT} set to 0.04 mg/ml and C_{PS-NH_2} set to somewhat above its saturation threshold without SWCNTs, an $E''(\omega)$ peak is noted; otherwise, with C_{PS-NH_2} set to below the threshold, no peak is noted at this C_{SWCNT} . Further, the peak position above PS-NH₂ saturation is approximately independent of C_{PS-NH_2} .

At 25°C, the terminal or Rouse relaxation time for a hypothetical unentangled 2,800 g/mol PS melt is ~ 0.006 s³⁹, more than an order-of-magnitude too small to explain the $E''(\omega)$ peak. Neat PS at this molecular weight is below its glass transition temperature, but solvation by toluene reduces this temperature and speeds up relaxation compared to the neat melt, and so the presence of toluene cannot explain the observed downward ω shift. Association of PS-NH₂ chain ends to SWCNTs presents a more likely explanation, as overall PS-NH₂ mobility is thereby reduced and PS tails are compelled to pack between SWCNTs. By dielectric spectroscopy and dynamic rheology, Kim et al. studied relaxation of polyisoprene tethered to nanoparticles, and at low molecular weight, they discovered a striking upturn in the relaxation time ratio between tethered and untethered chains.⁴⁰ The upturn's magnitude reaches several orders-of-magnitude, more than sufficient to realize the shifted $E''(\omega)$ peak position in the co-assembled film. Kim et al. suggested that this type of slowing for short chains was due to "tube-confinement by crowding". The rearrangement of PS-NH₂ between interfacial states in which the polymer is alternately bound and released from SWCNT presents an alternate explanation for the fast relaxation, assuming that unbound polymer confined to the interface can relax. While this rearrangement

mechanism is not entirely distinct from the crowding mechanism, given the weak interfacial activity of PS-NH₂ absent SWCNTs in the aqueous phase, an unbound PS-NH₂ population must be small. Also, the trend in relaxation peak position with C_{SWCNT} is most readily interpreted as a crowding effect.

Accepting the crowding argument, denser tethered PS-NH₂ should display slower relaxations, downshifting the $E''(\omega)$ peak position. Figure 5, displaying $E''(\omega)$ for films created at different pH, shows the predicted trend; as pH drops and more PS-NH₂ segregates to the interface, increased crowding of PS tails pushes the maximum of $E''(\omega)$ to lower ω . Lesser toluene in the denser film may further the downward trend. At pH 5.7 and above, where PS-NH₂ and SWCNTs are only weakly associated, $E''(\omega)$ for the co-assembled film is indistinguishable from $E''(\omega)$ for the pure PS-NH₂-coated oil/water interface, and although not observed, a peak at ω above the experimentally accessible range can be anticipated. Densification of PS-NH₂ was alternately achieved by abrupt contraction of drop surface area after equilibration at C_{PS-NH_2} below saturation (equilibration at 0.05 mg/ml), as displayed in Figure S6. Upon the contraction, $E'(\omega)$ rises across the ω range above the $E''(\omega)$ peak, but not below, and this peak is shifted downward, more so at larger contraction levels.

Slow Relaxation: Stress Relaxation after Step Strain. Slow interfacial relaxations, those at timescales too long to probe in a dynamics experiment and extending into the terminal relaxation regime, are readily accessed by a stress relaxation after step strain experiment. Figure 6 displays $E(t)$ after the sudden infinitesimal dilation of a drop equilibrated at $C_{SWCNT}=0.08$ mg/ml and $C_{PS-NH_2}=0.2$ mg/ml. The initial $E(t)$ value, ~ 50 mN/m, corresponds well to the high frequency plateau of $E'(\omega)$ determined in the equivalent dynamics experiment (see Figure 2a), suggesting that the fast PS-NH₂ structural relaxation is again captured, followed by a much slower relaxation below the frequency range spanned in the dynamics experiment. A double exponential decay well fits the curve, with a characteristic nominal fast relaxation time τ_1 of ~ 10 -15 s and a characteristic nominal slow relaxation time τ_2 of ~ 600 s. The former is consistent with PS-NH₂ structural relaxation, while the latter falls into the range of the longer adsorption/desorption (attachment/detachment) time outlined earlier. The fast relaxation time extracted from $E(t)$ curves grows from ~ 7 s to ~ 15 s as C_{SWCNT} increases from 0.02 mg/ml to 0.08 mg/ml, matching the downward shift in ω for the $E''(\omega)$ peak created by the PS-NH₂ relaxation. That the long relaxation time does not exactly match the times for adsorption/desorption (attachment/detachment) is not surprising, as the different experiments will weigh the underlying relaxation time distribution differently, accounting for order unity differences.

Eventually, $E(t)$ decays to ~ 0.3 mN/m for all SWCNT and PS-NH₂ concentrations studied, and in this equilibrium modulus limit, the measurement departs from zero only to within experimental error. Thus, under all conditions examined, although the longest relaxation is lengthy, full recovery is attainable, revealing that the co-assembled interfacial films are inherently fluid-like, buttressing the conclusion reached from the image sequence of the inset to **Figure 3**.

Conclusions

The dynamics of SWCNT/PS-NH₂ composite interfacial films was characterized by dilatational pendant drop rheometry, with two discrete relaxations identified along with an intermediate span of frequency/time following power-law relaxation behavior. As demonstrated in Figure 7, the fast relaxation was assigned to confinement-mediated Rouse-like chain dynamics of end-attached PS-NH₂ whereas the slow relaxation was ascribed to adsorption/desorption (attachment/detachment), a process that couples the dynamics of PS-NH₂ and SWCNTs. The reversibility of adsorption/desorption over the long relaxation timescale ultimately endows the films with fluid-like terminal behavior, although viscoelasticity is dominant across short timescales, those from seconds to tens of minutes. This rheological understanding can provide valuable guidance in tuning film mechanical properties for later membrane development. Moreover, the dynamics uncovered here carry over to other composite interfacial films made similarly, i.e., made by coupling at the oil/water interface of an oil-soluble hydrophobic polymeric amine with a water-soluble multi-carboxylated hydrophilic nanoparticle, and in particular, coupling appears to create fluid-like interfacial films whenever the polymeric amine is monofunctional. A different outcome might be expected for coupling with multi-functional polymeric amines, as in this case, the interfacial films can be physically crosslinked. Although the described interfacial co-assembly strategy is simple and highly flexible in regard to materials employed, the resultant film morphologies remain poorly characterized, with interfacial rheometry providing the best insights to date. Scattering and microscopy evaluations to complement the rheometry findings will help advance film applications, which are likely to manifest significantly the arrangement of components within the film.

Acknowledgments

The University of Massachusetts Materials Science and Engineering Center (MRSEC DMR-0820506) partially funded T.F. as well as the Shared Experimental Facilities that were used in conducting the research. TPR received partial support from LDRD at the Lawrence Berkeley National Laboratory.

References

1. Kalra, A.; Garde, S.; Hummer, G., Osmotic water transport through carbon nanotube membranes. *Proceedings of the National Academy of Sciences* **2003**, *100*, 10175-10180.
2. Thomas, J. A.; McGaughey, A. J., Reassessing fast water transport through carbon nanotubes. *Nano letters* **2008**, *8*, 2788-2793.
3. Falk, K.; Sedlmeier, F.; Joly, L.; Netz, R. R.; Bocquet, L., Molecular origin of fast water transport in carbon nanotube membranes: superlubricity versus curvature dependent friction. *Nano letters* **2010**, *10*, 4067-4073.
4. Hinds, B. J.; Chopra, N.; Rantell, T.; Andrews, R.; Gavalas, V.; Bachas, L. G., Aligned multiwalled carbon nanotube membranes. *Science* **2004**, *303*, 62-65.
5. Majumder, M.; Chopra, N.; Hinds, B. J., Effect of tip functionalization on transport through vertically oriented carbon nanotube membranes. *Journal of the American Chemical Society* **2005**, *127*, 9062-9070.
6. Boker, A.; Lin, Y.; Chiapperini, K.; Horowitz, R.; Thompson, M.; Carreon, V.; Xu, T.; Abetz, C.; Skaff, H.; Dinsmore, A. D.; Emrick, T.; Russell, T. P., Hierarchical nanoparticle assemblies formed by decorating breath figures. *Nat Mater* **2004**, *3*, 302-306.
7. Cui, M.; Emrick, T.; Russell, T. P., Stabilizing Liquid Drops in Nonequilibrium Shapes by the Interfacial Jamming of Nanoparticles. *Science* **2013**, *342*, 460-463.
8. He, J.; Niu, Z.; Tangirala, R.; Wang, J.-Y.; Wei, X.; Kaur, G.; Wang, Q.; Jutz, G.; Böker, A.; Lee, B.; Pingali, S. V.; Thiyagarajan, P.; Emrick, T.; Russell, T. P., Self-Assembly of Tobacco Mosaic Virus at Oil/Water Interfaces. *Langmuir* **2009**, *25*, 4979-4987.
9. Lin, Y.; Skaff, H.; Emrick, T.; Dinsmore, A. D.; Russell, T. P., Nanoparticle Assembly and Transport at Liquid-Liquid Interfaces. *Science* **2003**, *299*, 226-229.
10. Feng, T.; Hoagland, D. A.; Russell, T. P., Assembly of Acid-Functionalized Single-Walled Carbon Nanotubes at Oil/Water Interfaces. *Langmuir* **2014**, *30*, 1072-1079.
11. Hobbie, E. K.; Bauer, B. J.; Stephens, J.; Becker, M. L.; McGuiggan, P.; Hudson, S. D.; Wang, H., Colloidal Particles Coated and Stabilized by DNA-Wrapped Carbon Nanotubes. *Langmuir* **2005**, *21*, 10284-10287.
12. Sun, Z.; Feng, T.; Russell, T. P., Assembly of Graphene Oxide at Water/Oil Interfaces: Tessellated Nanotiles. *Langmuir* **2013**, *29*, 13407-13413.
13. Maestro, A.; Rio, E.; Drenckhan, W.; Langevin, D.; Salonen, A., Foams stabilised by mixtures of nanoparticles and oppositely charged surfactants: relationship between bubble shrinkage and foam coarsening. *Soft Matter* **2014**, *10*, 6975-6983.
14. Kim, H.; Jang, Y. R.; Yoo, J.; Seo, Y.-S.; Kim, K.-Y.; Lee, J.-S.; Park, S.-D.; Kim, C.-J.; Koo, J., Morphology Control of Surfactant-Assisted Graphene Oxide Films at the Liquid-Gas Interface. *Langmuir* **2014**, *30*, 2170-2177.
15. Maas, M.; Ooi, C. C.; Fuller, G. G., Thin Film Formation of Silica Nanoparticle/Lipid Composite Films at the Fluid-Fluid Interface. *Langmuir* **2010**, *26*, 17867-17873.
16. Whitby, C. P.; Fornasiero, D.; Ralston, J.; Liggieri, L.; Ravera, F., Properties of Fatty Amine-Silica Nanoparticle Interfacial Layers at the Hexane-Water Interface. *The Journal of Physical Chemistry C* **2012**, *116*, 3050-3058.

17. Krishnaswamy, R.; Majumdar, S.; Ganapathy, R.; Agarwal, V. V.; Sood, A. K.; Rao, C. N. R., Interfacial Rheology of an Ultrathin Nanocrystalline Film Formed at the Liquid/Liquid Interface. *Langmuir* **2007**, *23*, 3084-3087.
18. Ravera, F.; Ferrari, M.; Liggieri, L.; Loglio, G.; Santini, E.; Zanobini, A., Liquid-liquid interfacial properties of mixed nanoparticle-surfactant systems. *Colloids and Surfaces A: Physicochemical and Engineering Aspects* **2008**, *323*, 99-108.
19. Díez-Pascual, A. M.; Monroy, F.; Ortega, F.; Rubio, R. G.; Miller, R.; Noskov, B. A., Adsorption of Water-Soluble Polymers with Surfactant Character. Dilational Viscoelasticity. *Langmuir* **2007**, *23*, 3802-3808.
20. Wang, Y.-Y.; Dai, Y.-H.; Zhang, L.; Luo, L.; Chu, Y.-P.; Zhao, S.; Li, M.-Z.; Wang, E.-J.; Yu, J.-Y., Hydrophobically Modified Associating Polyacrylamide Solutions: Relaxation Processes and Dilational Properties at the Oil-Water Interface. *Macromolecules* **2004**, *37*, 2930-2937.
21. Freer, E. M.; Yim, K. S.; Fuller, G. G.; Radke, C. J., Interfacial rheology of globular and flexible proteins at the hexadecane/water interface: comparison of shear and dilatation deformation. *The Journal of Physical Chemistry B* **2004**, *108*, 3835-3844.
22. Freer, E. M.; Yim, K. S.; Fuller, G. G.; Radke, C. J., Shear and Dilatational Relaxation Mechanisms of Globular and Flexible Proteins at the Hexadecane/Water Interface. *Langmuir* **2004**, *20*, 10159-10167.
23. Erni, P.; Windhab, E. J.; Gunde, R.; Graber, M.; Pfister, B.; Parker, A.; Fischer, P., Interfacial Rheology of Surface-Active Biopolymers: Acacia senegal Gum versus Hydrophobically Modified Starch. *Biomacromolecules* **2007**, *8*, 3458-3466.
24. Imperiali, L.; Liao, K.-H.; Clasen, C.; Fransaer, J.; Macosko, C. W.; Vermant, J., Interfacial rheology and structure of tiled graphene oxide sheets. *Langmuir* **2012**, *28*, 7990-8000.
25. Reynaert, S.; Moldenaers, P.; Vermant, J., Interfacial rheology of stable and weakly aggregated two-dimensional suspensions. *Physical Chemistry Chemical Physics* **2007**, *9*, 6463-6475.
26. Madivala, B.; Fransaer, J.; Vermant, J., Self-assembly and rheology of ellipsoidal particles at interfaces. *Langmuir* **2009**, *25*, 2718-2728.
27. Freer, E. M.; Yim, K. S.; Fuller, G. G.; Radke, C. J., Interfacial Rheology of Globular and Flexible Proteins at the Hexadecane/Water Interface: Comparison of Shear and Dilatation Deformation. *The Journal of Physical Chemistry B* **2004**, *108*, 3835-3844.
28. Ravera, F.; Santini, E.; Loglio, G.; Ferrari, M.; Liggieri, L., Effect of Nanoparticles on the Interfacial Properties of Liquid/Liquid and Liquid/Air Surface Layers. *The Journal of Physical Chemistry B* **2006**, *110*, 19543-19551.
29. Pauchard, V.; Rane, J. P.; Banerjee, S., Asphaltene-Laden Interfaces Form Soft Glassy Layers in Contraction Experiments: A Mechanism for Coalescence Blocking. *Langmuir* **2014**, *30*, 12795-12803.
30. Sun, H.-Q.; Zhang, L.; Li, Z.-Q.; Zhang, L.; Luo, L.; Zhao, S., Interfacial dilational rheology related to enhance oil recovery. *Soft Matter* **2011**, *7*, 7601-7611.
31. Saien, J.; Akbari, S., Interfacial Tension of Toluene + Water + Sodium Dodecyl Sulfate from (20 to 50) °C and pH between 4 and 9. *Journal of Chemical & Engineering Data* **2006**, *51*, 1832-1835.
32. Laurent, C.; Flahaut, E.; Peigney, A., The weight and density of carbon nanotubes versus the number of walls and diameter. *Carbon* **2010**, *48*, 2994-2996.

33. Winter, H. H.; Chambon, F., Analysis of Linear Viscoelasticity of a Crosslinking Polymer at the Gel Point. *Journal of Rheology* **1986**, *30*, 367-382.
34. Winter, H. H.; Chambon, F., Analysis of Linear Viscoelasticity of a Crosslinking Polymer at the Gel Point. *Journal of Rheology (1978-present)* **1986**, *30*, 367-382.
35. Hou, L.; Zhang, Q.; Ling, L.; Li, C.-X.; Chen, L.; Chen, S., Interfacial fabrication of single-crystalline ZnTe nanorods with high blue fluorescence. *Journal of the American Chemical Society* **2013**, *135*, 10618-10621.
36. Lee, K. Y.; Kim, M.; Hahn, J.; Suh, J. S.; Lee, I.; Kim, K.; Han, S. W., Assembly of metal nanoparticle-carbon nanotube composite materials at the liquid/liquid interface. *Langmuir* **2006**, *22*, 1817-1821.
37. Marsh, D. H.; Rance, G. A.; Whitby, R. J.; Giustiniano, F.; Khlobystov, A. N., Assembly, structure and electrical conductance of carbon nanotube-gold nanoparticle 2D heterostructures. *Journal of Materials Chemistry* **2008**, *18*, 2249-2256.
38. He, J.; Zhang, Q.; Gupta, S.; Emrick, T.; Russell, T. P.; Thiyagarajan, P., Drying droplets: a window into the behavior of nanorods at interfaces. *Small* **2007**, *3*, 1214-1217.
39. Stratton, R. A., Non-Newtonian flow in polymer systems with no entanglement coupling. *Macromolecules* **1972**, *5*, 304-310.
40. Agarwal, P.; Kim, S. A.; Archer, L. A., Crowded, Confined, and Frustrated: Dynamics of Molecules Tethered to Nanoparticles. *Physical Review Letters* **2012**, *109*, 258301.

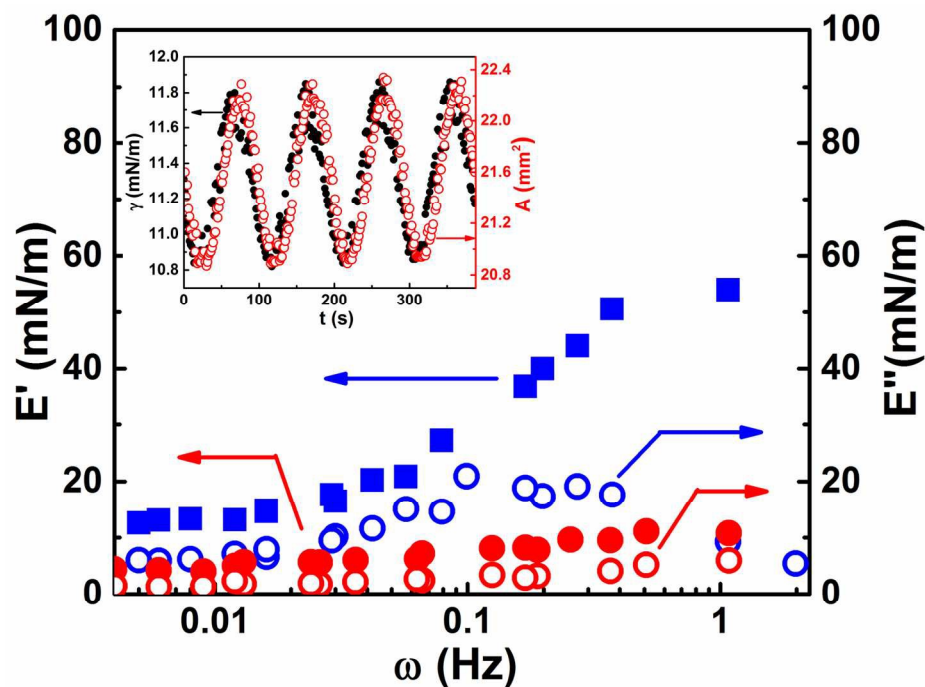


Figure 1. Storage and loss dilatational moduli, $E'(\omega)$ and $E''(\omega)$, for a pure PS-NH₂ film (red) and a SWCNTs/PS-NH₂ film (blue) measured by oscillatory pendant drop tensiometry/rheometry ($C_{SWCNT}=0.02$ mg/ml, $C_{PS-NH_2}=0.2$ mg/ml, PS-NH₂ $M_n \sim 2,800$ g/mol, pH=3.0). Inset: Underlying rheological data, i.e., oscillatory surface tension $\gamma(t)$ plotted alongside oscillatory drop area $A(t)$ at $\omega=0.01$ Hz.

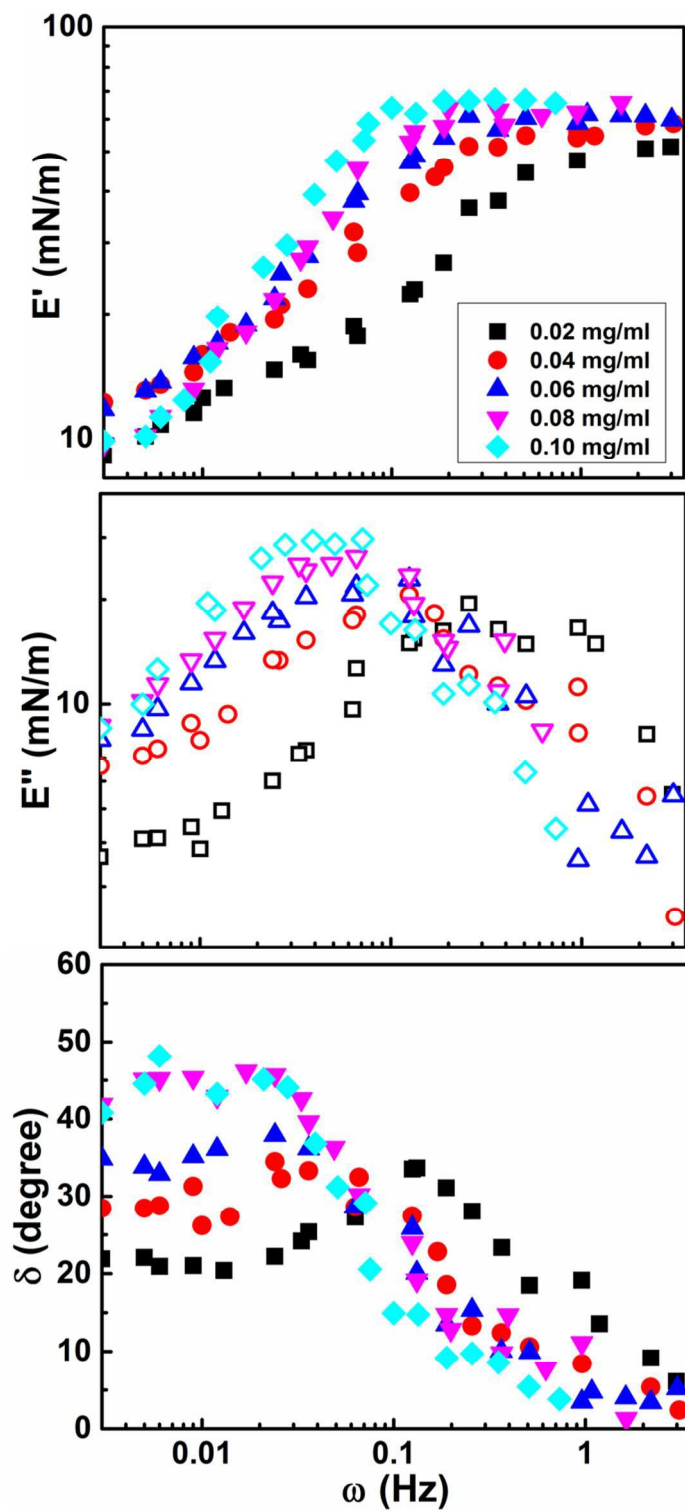


Figure 2. $E'(\omega)$, $E''(\omega)$, and $\delta(\omega)$ for various C_{SWCNT} ($C_{PS-NH_2}=0.2$ mg/ml, PS-NH₂ $M_n \sim 2,800$ g/mol, pH=3.0).

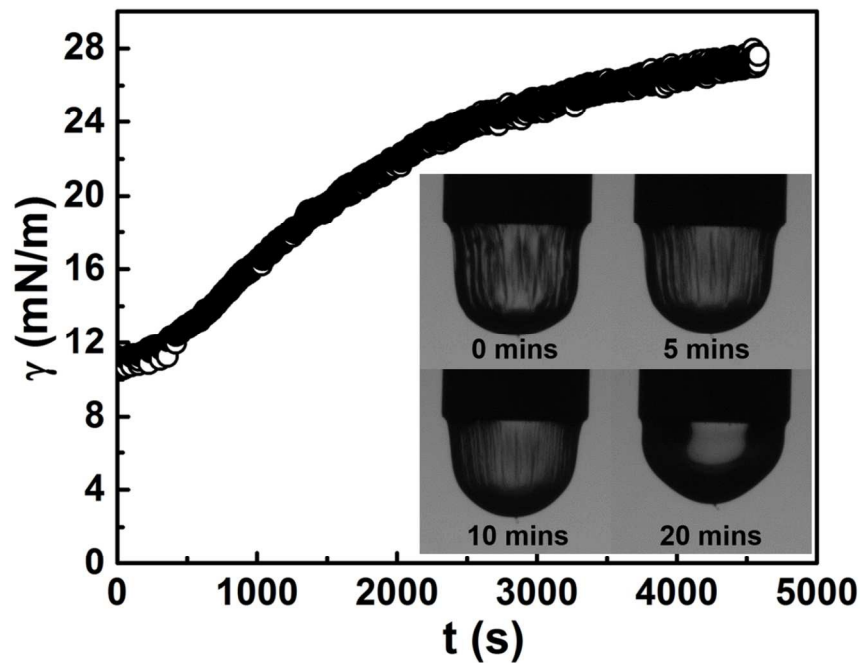


Figure 3. Recovery in $\gamma(t)$ after bulk PS-NH₂ in toluene is exchanged with bulk pristine toluene ($C_{SWCNT}=0.02$ mg/ml, $C_{PS-NH_2}=0.2$ mg/ml, PS-NH₂ $M_n \sim 2,800$ g/mol, pH=3.0). Inset: images of wrinkle recovery after an abrupt, large amplitude dilatational compression.

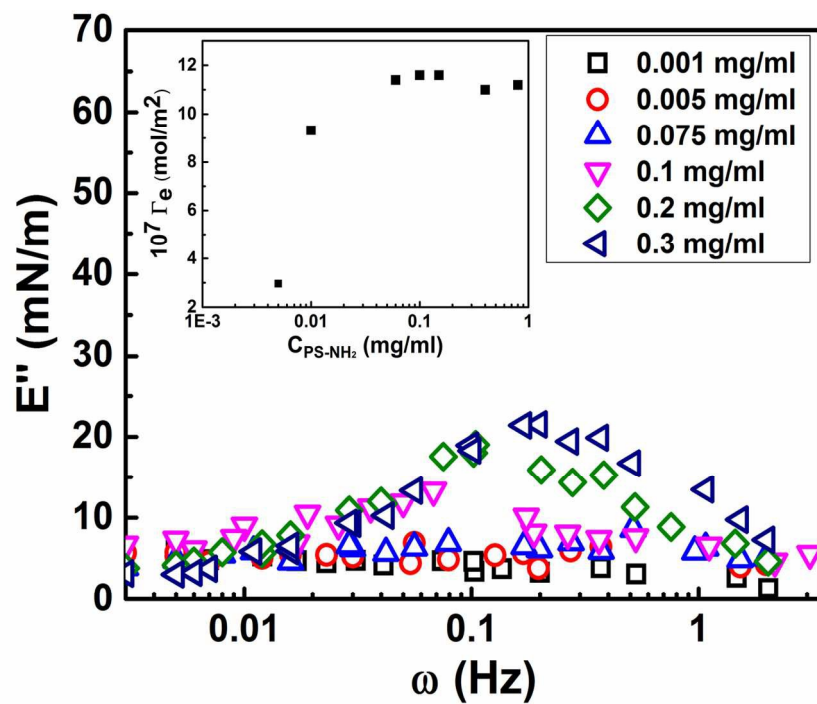


Figure 4. $E''(\omega)$ for various C_{PS-NH_2} ($C_{SWCNT}=0.04$ mg/ml, pH=3.0). Inset: PS-NH₂ surface excess Γ_{PS-NH_2} measured by the Gibb's absorption isotherm method for various C_{PS-NH_2} when SWCNTs are absent from the aqueous phase.

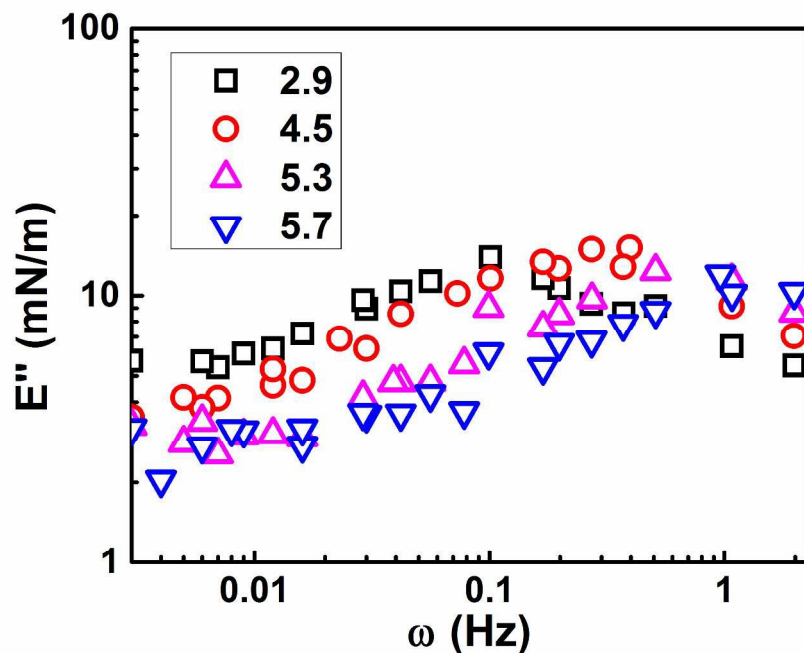


Figure 5. pH dependence of $E''(\omega)$ ($C_{SWCNT}=0.04$ mg/ml, $C_{PS-NH_2}=0.2$ mg/ml, PS-NH₂ $M_n \sim 2,800$ g/mol, pH=3.0).

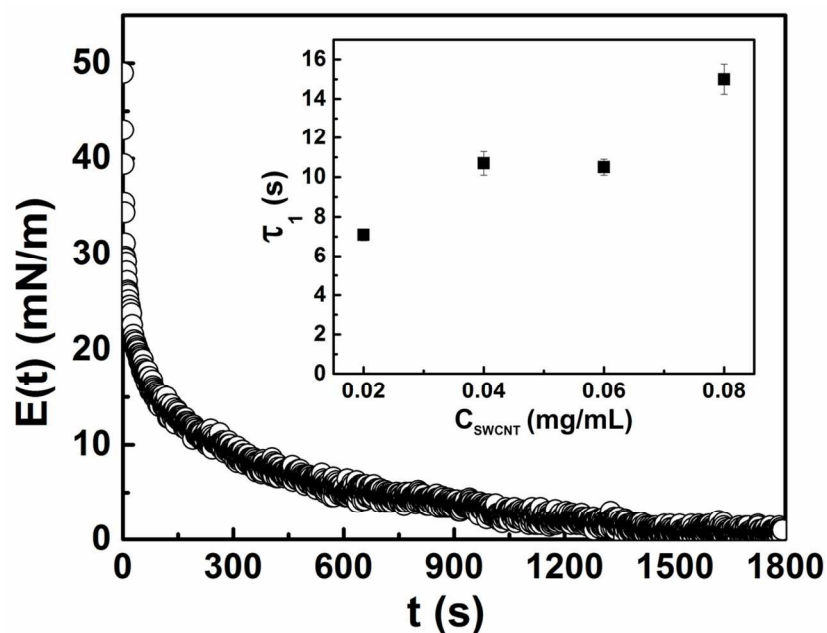


Figure 6. Dilatational relaxation modulus $E(t)$ for a co-assembled SWCNT/PS-NH₂ film ($C_{SWCNT}=0.08$ mg/ml, $C_{PS-NH_2}=0.2$ mg/ml, PS-NH₂ $M_n \sim 2,800$ g/mol, pH=3.0). Inset: Fast relaxation time τ_1 extracted from $E(t)$ as a function of C_{SWCNT} .

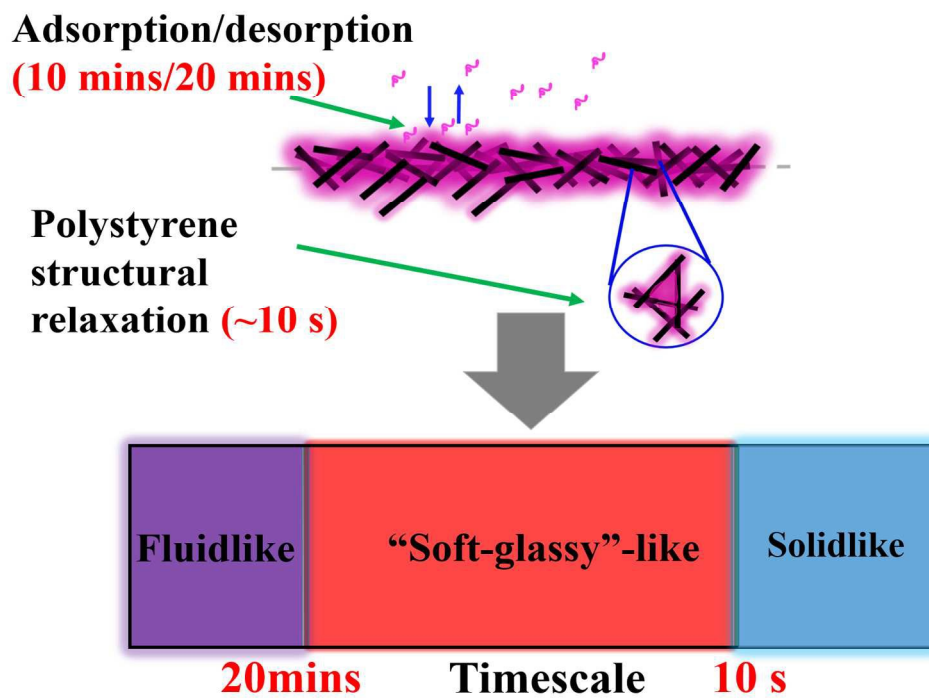
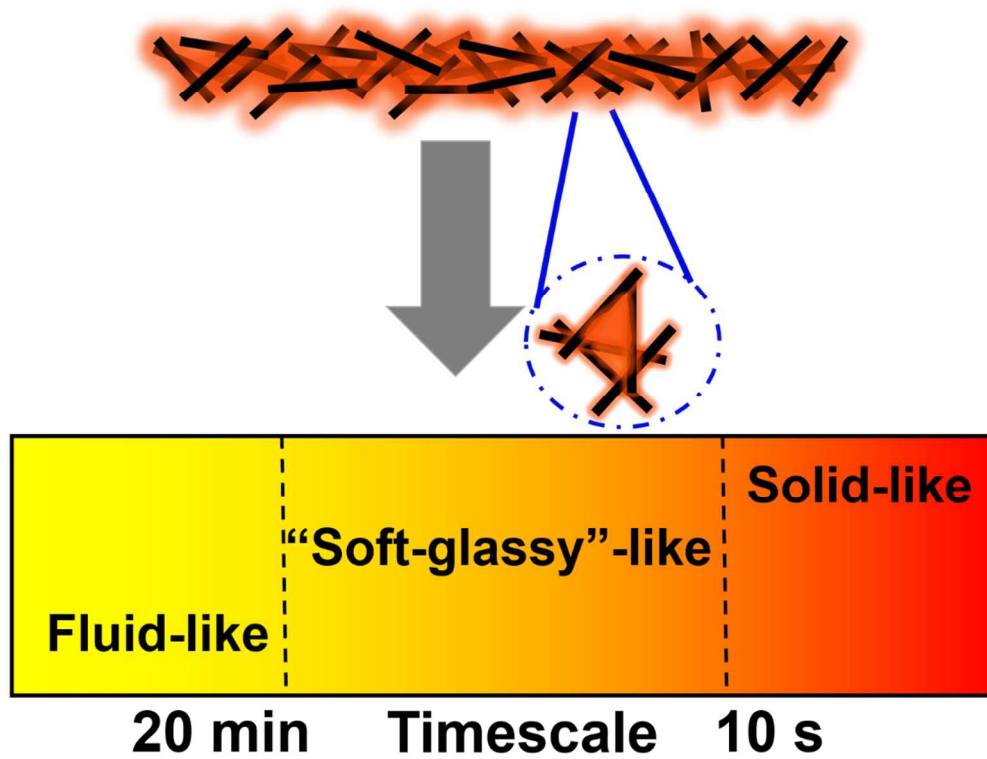


Figure 7. Relaxations identified for SWCNT/PS-NH₂ composite co-assembled interfacial films.



Rheology of nanoscale composite thin-films at liquid/liquid interfaces